A Low-Energy-Gap Organic Dye for High-Performance Small-Molecule Organic Solar Cells

Li-Yen Lin,[†] Yi-Hong Chen,[‡] Zheng-Yu Huang,[‡] Hao-Wu Lin,*[‡] Shu-Hua Chou,[†] Francis Lin,[†] Chang-Wen Chen,[‡] Yi-Hung Liu,[†] and Ken-Tsung Wong*[†]

[†]Department of Chemistry, National Taiwan University, Taipei 10617, Taiwan
[‡]Department of Materials Science and Engineering, National Tsing Hua University, Hsin Chu 30013, Taiwan

S Supporting Information

ABSTRACT: A novel donor−acceptor−acceptor (D−A−A) donor molecule, **DTDCTB**, in which an electron-donating ditolylaminothienyl moiety and an electron-withdrawing dicyanovinylene moiety are bridged by another electron-accepting 2,1,3-benzothiadiazole block, has been synthesized and characterized. A vacuum-deposited organic solar cell employing **DTDCTB** combined with the electron acceptor C_{70} achieved a record-high power conversion efficiency (PCE) of 5.81%. The respectable PCE is attributed to the solar spectral response extending to the near-IR region and the ultracompact absorption dipole stacking of the **DTDCTB** thin film.

Organic solar cells (OSCs) have garnered considerable research interest because of their prominent merits, such as low cost, light weight, and mechanical flexibility. At present, solution-processed bulk heterojunction (BHJ) solar cells[1] based on bicontinuous interpenetrating networks of π-conjugated polymers and soluble fullerene derivatives have demonstrated remarkable achievements, with power conversion efficiencies (PCEs) in excess of 7%.[2] Beyond that, the small-molecule counterparts, particularly p-type organic semiconductors utilized for OSCs, have also shown exceptional promise. The competitive nature of small molecules relative to polymeric materials can be ascribed to the predominant advantages including well-defined molecular structures, easier purification, and better batch-to-batch reproducibility. Therefore, tremendous research endeavors have been devoted to developing small-molecule OSCs (SMOSCs),[3] which exhibit appreciable PCEs of >5%, by using either solution-processing or vacuum-deposition fabrication techniques.[4] Although solution processing is generally considered to be more cost-effective than vacuum deposition, vacuum-deposited SMOSCs are emerging as competitive OSCs because of the advantage of easy fabrication of multilayer tandem architectures.[5] In this regard, a tandem SMOSC device with a PCE of up to 8.3% has been disclosed recently.[6]

To date, the molecular architectures of most donor materials for SMOSCs fabricated by vacuum-evaporation processes can be classified into two main categories: acceptor−donor−acceptor (A−D−A) and donor−acceptor (D−A) systems. A−D−A systems, in which electron-rich oligothiophenes are end-capped with various electron-withdrawing groups such as dicyanovinylene, 2,1,3-benzothiadiazole, and thiadiazolo[3,4-c]pyridine, are currently among the most successful molecular architectures.

Tailoring of the conjugation length of the oligothiophene core unit as well as the length and location of pendant alkyl side chains has enabled this class of active materials to demonstrate reliable PCEs.[7] One distinctive feature of such materials is that they possess deep-lying highest occupied molecular orbital (HOMO) energy levels and thus afford SMOSCs with extraordinary open-circuit voltages (V_{oc}) of ∼1 V. On the other hand, D−A-type molecules incorporating arylamines as electron-donating groups also appear to be attractive candidates because of their effective intramolecular charge transfer (ICT) characteristics. Moreover, taking advantage of the versatility of structural modifications in such systems enables the frontier orbital energy levels to be readily tuned through judicious combinations of different electron-donating and/or -accepting functional groups. Along this line, a series of triphenylamine-based D−A materials have been reported to exhibit PCEs of up to 2.2%.[8] However, both of these types of materials generally suffer from insufficient light-harvesting capabilities. They usually have absorption maxima at less than 600 nm, which may be one of the main impediments to further improvement of their efficiencies. Although a few dyes, such as squaraine[9] and merocyanine,[10] have been explored to address this issue, the progress still lags behind that for the A−D−A counterparts. Therefore, it is highly desired to design new molecular architectures that can readily allow donor materials to extend the spectral responses to the far-red and even near-IR regions.

In this communication, we report a novel donor−acceptor−acceptor (D−A−A)-type donor molecule, **DTDCTB** (Scheme 1), whose thin-film absorption can extend into the near-IR region. In this molecule, an electron-donating ditolylaminothienyl moiety and an electron-withdrawing dicyanovinylene moiety are bridged by another electron-accepting 2,1,3-benzothiadiazole (BT) block. Specifically, **DTDCTB** was designed with the following structural characteristics: (i) The ditolylaminothienyl block behaves as a stronger electron-donating moiety in comparison with the conventional ditolylaminophenyl congener because of its fortified quinoidal character. The quinoidal resonance structure is energetically less stable than the aromatic form, and thus, the adoption of the ditolylaminothienyl donor endows **DTDCTB** with a smaller band gap.[1c] (ii) The BT moiety represents the most ubiquitous acceptor utilized in optoelectronic materials (e.g., low-band-gap polymer donors,[1] nonfullerene acceptors,[11] and n-type field-effect transistors[12]) because of its fascinating features, including low-

Scheme 1. Synthetic Route to DTDCTB[a]
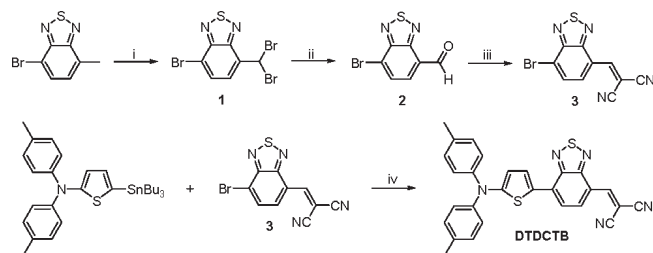
[a] (i) NBS, azobis(isobutyronitrile), chlorobenzene, 80 °C, 83%. (ii) AgNO₃, H₂O/MeCN, reflux, 92%. (iii) Malononitrile, Al₂O₃, toluene, 70 °C, 67%. (iv) PdCl₂(PPh₃)₂, toluene, 110 °C, 55%.
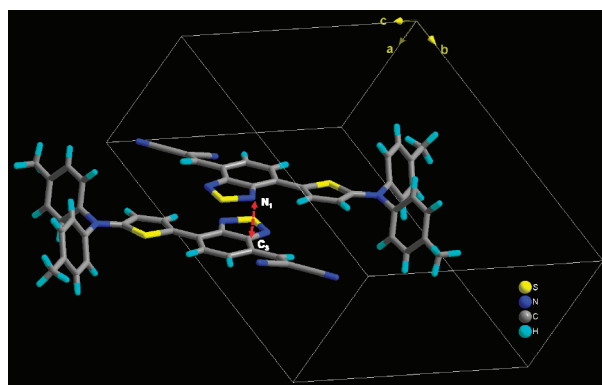

Figure 1. X-ray-analyzed molecular structure and crystal packing of **DTDCTB**.

Figure 2. Cyclic voltammograms of **DTDCTB** in solution.

Figure 3. (a) Normalized absorption spectra of **DTDCTB** in CH₂Cl₂ and a thin film. (b) Optical constants (refractive index, n, and extinction coefficient, k) of **DTDCTB**, C_{60}, and C_{70} thin-film spectra.

band-gap character, high absorption coefficient, and appropriate energy levels. (iii) According to our previous study,[13] the innovative combination of two acceptors (BT and dicyanovinylene used here) would effectively narrow the optical band gap of the resulting molecule while maintaining a relatively low-lying HOMO energy level, and thus, an enhanced short-circuit current (J_{sc}) and V_{oc} value can be concurrently anticipated. As a proof of concept, our preliminary investigation of vacuum-deposited SMOSCs employing **DTDCTB** as the electron donor and C_{70} as the electron acceptor revealed a remarkable PCE as high as 5.81%. To the best of our knowledge, this efficiency is among the highest values ever reported for vacuum-deposited single cells with organic donor molecules. This encouraging result indicates the great potential of such D–A–A systems in creating high-performance donor materials for SMOSCs.

The synthesis of **DTDCTB** is described in Scheme 1. Benzylic bromination of 4-bromo-7-methyl-2,1,3-benzothiadiazole[14] with *N*-bromosuccinimide (NBS) afforded **1**. Silver nitrate-promoted hydrolysis of **1** gave aldehyde **2**, which was then condensed with malononitrile to give the key intermediate **3** via Knöevenagel reaction in the presence of basic Al₂O₃. Finally, Stille coupling of 5-(*N*,*N*-ditolylamino)-2-(tri-*n*-butylstannyl)thiophene[15] and **3** yielded **DTDCTB** in good yield. It is noteworthy that this synthetic route provides a versatile method for further engineering of the molecular structure through the combination of the unsymmetrical intermediate **3** and other electron-donating groups.

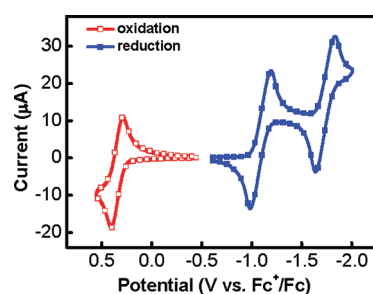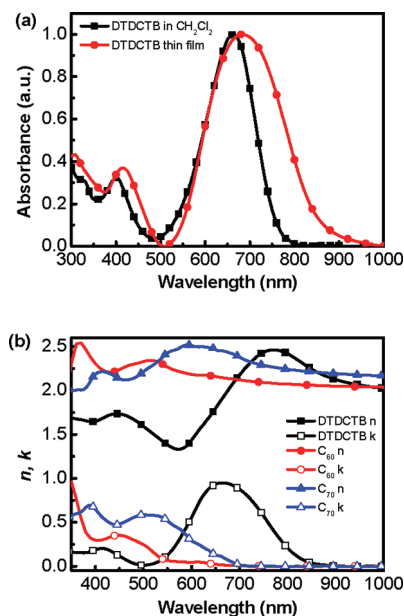The molecular structure of **DTDCTB** was analyzed by X-ray crystallography. As shown in Figure 1, **DTDCTB** displays an almost coplanar conformation between the thiophene and BT rings with a dihedral angle of 5.5°. This coplanarity facilitates the electronic coupling between the electron-donating and electron-withdrawing blocks, enhancing the ICT efficiency and thus ensuring a distinctive bathochromic shift of the spectral responses. The strong polar character and coplanar conformation of the heteroaryl components lead **DTDCTB** crystals to pack in an antiparallel manner along both molecular axis directions. The cofacial arrangement of two neighboring BT rings with a shortest point-to-point (N1–C3) distance of 3.55 Å indicates non-negligible π–π interactions, which may facilitate charge-carrier hopping in the solid state.

The electrochemical properties of **DTDCTB** were probed by cyclic voltammetry in solution. As shown in Figure 2, **DTDCTB** exhibits one reversible oxidation potential at 0.35 V vs ferrocene/ferrocenium (Fc/Fc⁺), corresponding to oxidation of the ditolylaminothienyl donor. On the other hand, two reversible reduction waves at −1.09 and −1.74 V vs Fc/Fc⁺ were observed in the cathodic potential regime. The first reduction potential can be ascribed to the reduction of the dicyanovinylene block and the second to reduction of the BT fragment. By reference to the Fc/Fc⁺ redox couple, where the HOMO of Fc is assigned to be 4.8 eV below the vacuum level, the HOMO and lowest

unoccupied molecular orbital (LUMO) energy levels of **DTDCTB** were calculated to be −5.15 and −3.71 eV on the basis of the oxidation potential and the first reduction potential, respectively. In spite of the presence of the strong ditolylaminothienyl donor, **DTDCTB** shows a relatively low-lying HOMO level because of the strong electron-withdrawing character of the BT and dicyanovinylene blocks. Given energy level shifts due to intermolecular interactions, the HOMO level of the **DTDCTB** thin film was determined by UV photoelectron spectroscopy to have a value of −5.30 eV. The fairly low-lying HOMO would result in a large energy level offset to the LUMOs of fullerenes, ensuring relatively large V_{oc} values.

Figure 3a shows the electronic absorption spectra of **DTDCTB** in a vacuum-deposited thin film and in CH_2Cl_2 solution. Surprisingly, with such a short effective conjugation length, the absorption spectrum of **DTDCTB** in solution shows a band at λ_{max} = 663 nm accompanied by a high extinction coefficient (k) of up to 41 660 M^{-1} cm^{-1}. To gain more insight into the electronic and optical properties of **DTDCTB**, density functional theory (DFT) and time-dependent DFT (TDDFT) calculations were performed for the molecule in CH_2Cl_2 solution [Figure S1 and Tables S1 and S2 in the Supporting Information (SI)] and gave a computed λ_{max} value of 673 nm that is close to the experimental results. On the other hand, the thin-film absorption of **DTDCTB** exhibits λ_{max} = 684 nm. The significant broadening of the thin-film absorption spectrum is possibly due to intermolecular $\pi-\pi$ stacking as evidenced in the crystal packing. Apparently, the thin-film absorption of **DTDCTB** effectively extends the useful photon-harvesting range down to near-IR wavelengths (700−800 nm). Optical constants of vacuum-deposited thin films of **DTDCTB**, C_{60}, and C_{70} are shown in Figure 3b. The **DTDCTB** thin film exhibits high k values across the 550−800 nm wavelength range, with $k_{max} \approx 0.95$ at λ = 670 nm, which is coincident with the absorption spectrum shown in Figure 3a. Notably, the k_{max} value is among the highest reported for solar-absorbing organic thin films, as compared with the commonly used nano/microcrystalline poly(3-hexylthiophene) (P3HT) and copper phthalocyanine (CuPc), which show k_{max} values of ∼0.65 and ∼0.95, respectively.[16,17] This result indicates that the efficient ICT gives the **DTDCTB** molecule high polar character, which favors the formation of ultracompact absorption dipole packing in the thin film upon vacuum deposition. In addition, the k spectra of the commonly used acceptor molecules C_{60} and C_{70} show complementary wavelength coverage (<550 nm) with respect to the **DTDCTB** thin film. As a result, fullerenes C_{60} and C_{70} were selected as acceptor materials to be paired with **DTDCTB** for subsequent device fabrication.

In photovoltaic characterizations, we adopted the vacuum-deposited planar mixed heterojunction (PMHJ) structure incorporating one layer of mixed donor/acceptor materials sandwiched between pure donor and acceptor layers.[18] The optimized device structures were configured as follows: Device I: ITO/MoO_3 (30 nm)/**DTDCTB** (7 nm)/1:1 (v/v) **DTDCTB**:C_{60} (40 nm)/C_{60} (20 nm)/ 2,9-dimethyl-4,7-diphenyl-1,10-phenanthroline (BCP) (10 nm)/Ag (150 nm). Device II: ITO/MoO_3 (5 nm)/**DTDCTB** (7 nm)/1:1 (v/v) **DTDCTB**:C_{70} (40 nm)/ C_{70} (7 nm)/BCP (10 nm)/Ag (150 nm). In these devices, BCP was employed as both an electron-transporting layer and an exciton-blocking layer. More importantly, MoO_3 was chosen as the hole-transporting layer because of its superior performance in comparison with several other hole-transporting materials.[19] It was noted that BHJ polymer solar cells incorporating MoO_3 usually
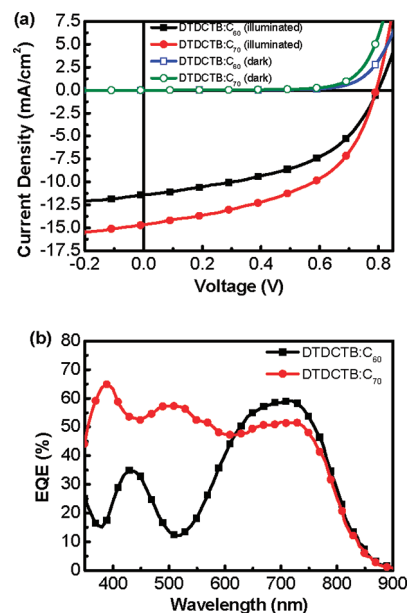
Figure 4. (a) $J-V$ characteristics and (b) EQE spectra of **DTDCTB**:C_{60} PMHJ (squares) and DTDCTB:C_{70} PMHJ (circles) solar cells.

exhibit better device stability than those fabricated with poly (3,4- ethylenedioxythiophene):poly(styrenesulfonate) (PEDOT: PSS).[20] Optimizations to fine-tune the thicknesses of the **DTDCTB** and MoO_3 layers are shown in the SI. It was found that the devices with a 7 nm **DTDCTB** donor layer demonstrated superior performance. Moreover, through spectrum-response modeling of the simplified bilayer cells, the exciton diffusion length in the **DTDCTB** thin film was found to be ∼6 nm (Figure S4),[21] which is within the typical range of 5−10 nm for organic semiconductors. Figure 4a shows the current density−voltage ($J-V$) characteristics of **DTDCTB**:fullerene PMHJ solar cells. The **DTDCTB**:C_{60} PMHJ device gave a V_{oc} of 0.80 V, a J_{sc} of 11.40 mA/cm^2, and fill factor (FF) of 0.48, yielding a PCE of 4.41% under AM 1.5 G 1 sun (100 mW/cm^2) simulated solar illumination. Remarkably, the **DTDCTB**:C_{70} device delivered higher performance, with a V_{oc} of 0.79 V, J_{sc} of 14.68 mA/cm^2, FF of 0.50, and PCE of 5.81%, which is the highest one ever reported for SMOSCs. The high V_{oc} values of these devices are due to the moderately low-lying HOMO level of **DTDCTB**. However, the V_{oc} value (∼0.8 V) still leaves room for future improvement. The FF values of the **DTDCTB**:C_{60} and **DTDCTB**:C_{70} devices are similar, suggesting similar blending layer morphologies and charge-carrier percolation networks in the two devices. The higher J_{sc} of the **DTDCTB**:C_{70} device can be attributed to the higher extinction coefficient of C_{70} relative to C_{60}, which is fully consistent with the external quantum efficiency (EQE) spectra shown in Figure 4b. The EQE spectrum of the **DTDCTB**:C_{70} device shows impressive high values of ∼50% throughout the UV−vis to near-IR range (350−770 nm), resulting in the high J_{sc}. It is noteworthy that the integrated EQE values are in agreement with the measured short-circuit currents (within 3−5% error; see Tables S3 and S4). Although the **DTDCTB**:C_{70} films show amorphous morphologies (see the X-ray diffractogram in Figure S5), the donor−acceptor phase separation can be clearly observed in the phase image of the **DTDCTB**:C_{70} film (Figure S6). The effective phase separation may provide carrier transportation pathways and contribute to high quantum efficiencies.

In conclusion, a novel D−A−A-type donor material, **DTDCTB**, in which an electron-donating ditolylaminothienyl moiety is connected to an electron-withdrawing dicyanovinylene moiety through another electron-accepting 2,1,3-benzothiadiazole block, has been synthesized and applied in the fabrication of vacuum-deposited SMOSCs. The innovative structural design strategy enables **DTDCTB** to exhibit distinguished light-harvesting abilities with spectral responses close to the near-IR region. A vacuum-deposited SMOSC employing **DTDCTB** as the electron donor and C_{70} as the electron acceptor demonstrated an exceptional PCE of up to 5.81% in initial trials. This efficiency is among the highest ever obtained for organic vacuum-deposited single cells. The high efficiency is primarily attributed to the broad and intensive absorption (giving high J_{sc}) and a reasonably low-lying HOMO level (giving high V_{oc}) of the **DTDCTB** thin film. Our results may advance efforts to develop new organic dyes to boost the device performance of SMOSCs.

■ ASSOCIATED CONTENT

ⓢ Supporting Information. Synthesis, characterization, copies of ^{1}H and ^{13}C NMR spectra, CIF for **DTDCTB**, procedures for fabricating devices and performing measurements, quantum-mechanical calculations, an atomic force microscopy image, and an X-ray diffractogram. This material is available free of charge via the Internet at http://pubs.acs.org.

■ AUTHOR INFORMATION

Corresponding Author
hwlin@mx.nthu.edu.tw; kenwong@ntu.edu.tw

■ ACKNOWLEDGMENT

■ REFERENCES

(1) (a) Yu, G.; Gao, J.; Hummelen, J. C.; Wudl, F.; Heeger, A. J. *Science* **1995**, *270*, 1789. (b) Thompson, B. C.; Fréchet, J. M. J. *Angew. Chem., Int. Ed.* **2008**, *47*, 58. (c) Cheng, Y.-J.; Yang, S.-H.; Hsu, C.-S. *Chem. Rev.* **2009**, *109*, 5868. (d) Wong, W. Y.; Ho, C. L. *Acc. Chem. Res.* **2010**, *43*, 1246. (e) Park, S. H.; Roy, A.; Beaupre, S.; Cho, S.; Coates, N.; Moon, J. S.; Moses, D.; Leclerc, M.; Lee, K.; Heeger, A. J. *Nat. Photonics* **2009**, *3*, 297. (f) Coffin, R. C.; Peet, J.; Rogers, J.; Bazan, G. C. *Nat. Chem.* **2009**, *1*, 657. (g) Huang, F.; Chen, K.-S.; Yip, H.-L.; Hau, S. K.; Acton, O.; Zhang, Y.; Luo, J. D.; Jen, A. K.-Y. *J. Am. Chem. Soc.* **2009**, *131*, 13886. (h) Huo, L. J.; Hou, J. H.; Zhang, S. Q.; Chen, H.-Y.; Yang, Y. *Angew. Chem., Int. Ed.* **2010**, *49*, 1500.

(2) (a) Liang, Y. Y.; Xu, Z.; Xia, J. B.; Tsai, S.-T.; Wu, Y.; Li, G.; Ray, C.; Yu, L. P. *Adv. Mater.* **2010**, *22*, E135. (b) Zhou, H. X.; Yang, L. Q.; Stuart, A. C.; Price, S. C.; Liu, S. B.; You, W. *Angew. Chem., Int. Ed.* **2011**, *50*, 2995. (c) Chu, T.-Y.; Lu, J. P.; Beaupre, S.; Zhang, Y. G.; Pouliot, J.-R.; Wakim, S.; Zhou, J. Y.; Leclerc, M.; Li, Z.; Ding, J. F.; Tao, Y. *J. Am. Chem. Soc.* **2011**, *133*, 4250. (d) Price, S. C.; Stuart, A. C.; Yang, L. Q.; Zhou, H. X.; You, W. *J. Am. Chem. Soc.* **2011**, *133*, 4625.

(3) (a) Walker, B.; Tamayo, A. B.; Dang, X. D.; Zalar, P.; Seo, J. H.; Garcia, A.; Tantiwiwat, M.; Nguyen, T. Q. *Adv. Funct. Mater.* **2009**, *19*, 3063. (b) Mikroyannidis, J. A.; Sharma, S. S.; Vijay, Y. K.; Sharma, G. D. *ACS Appl. Mater. Interfaces* **2010**, *2*, 270. (c) Walker, B.; Kim, C.;

Nguyen, T. Q. *Chem. Mater.* **2011**, *23*, 470. (d) Shang, H. X.; Fan, H. J.; Liu, Y.; Hu, W. P.; Li, Y. F.; Zhan, X. W. *Adv. Mater.* **2011**, *23*, 1554. (e) Loser, S.; Bruns, C. J.; Miyauchi, H.; Ortiz, R. P.; Facchetti, A.; Stupp, S. I.; Marks, T. J. *J. Am. Chem. Soc.* **2011**, *133*, 8142.

(4) (a) Wei, G. D.; Wang, S. Y.; Sun, K.; Thompson, M. E.; Forrest, S. R. *Adv. Energy Mater.* **2011**, *1*, 184. (b) Fitzner, R.; Reinold, E.; Mishra, A.; Mena-Osteritz, E.; Ziehlke, H.; Körner, C.; Leo, K.; Riede, M.; Weil, M.; Tsaryova, O.; Weiß, A.; Uhrich, C.; Pfeiffer, M.; Bäuerle, P. *Adv. Funct. Mater.* **2011**, *21*, 897. (c) Matsuo, Y.; Sato, Y.; Niinomi, T.; Soga, I.; Tanaka, H.; Nakamura, E. *J. Am. Chem. Soc.* **2009**, *131*, 16048.

(5) Drechsel, J.; Männig, B.; Kozlowski, F.; Pfeiffer, M.; Leo, K.; Hoppe, H. *Appl. Phys. Lett.* **2005**, *86*, No. 244102.

(6) Heliatek GmbH press release, Oct 11, 2010; http://www.heliatek.com.

(7) (a) Schulze, K.; Uhrich, C.; Schüppel, R.; Leo, K.; Pfeiffer, M.; Brier, E.; Reinold, E.; Bäuerle, P. *Adv. Mater.* **2006**, *18*, 2872. (b) Wynands, D.; Levichkova, M.; Leo, K.; Uhrich, C.; Schwartz, G.; Hildebrandt, D.; Pfeiffer, M.; Riede, M. *Appl. Phys. Lett.* **2010**, *97*, No. 073503. (c) Steinberger, S.; Mishra, A.; Reinold, E.; Levichkov, J.; Uhrich, C.; Pfeiffer, M.; Bäuerle, P. *Chem. Commun.* **2011**, *47*, 1982.

(8) (a) Roquet, S.; Cravino, A.; Leriche, P.; Alévêque, O.; Frère, P.; Roncali, J. *J. Am. Chem. Soc.* **2006**, *128*, 3459. (b) Cravino, A.; Leriche, P.; Alévêque, O.; Roquet, S.; Roncali, J. *Adv. Mater.* **2006**, *18*, 3033. (c) Hiroshi, H.; Ohishi, H.; Tanaka, M.; Ohmori, Y.; Shirota, Y. *Adv. Funct. Mater.* **2009**, *19*, 3948.

(9) Wang, S. Y.; Mayo, E. I.; Perez, M. D.; Griffe, L.; Wei, G. D.; Djurovich, P. I.; Forrest, S. R.; Thompson, M. E. *Appl. Phys. Lett.* **2009**, *94*, No. 233304.

(10) Kronenberg, N. M.; Steinmann, V.; Bürckstümmer, H.; Hwang, J.; Hertel, D.; Würthner, F.; Meerholz, K. *Adv. Mater.* **2010**, *22*, 4193.

(11) Schwenn, P. E.; Gui, K.; Nardes, A. M.; Krueger, K. B.; Lee, K. H.; Mutkins, K.; Rubinstein-Dunlop, H.; Shaw, P. E.; Kopidakis, N.; Burn, P. L.; Meredith, P. *Adv. Energy Mater.* **2011**, *1*, 73.

(12) Mutkins, K.; Gui, K.; Aljada, M.; Schwenn, P. E.; Namdas, E. B.; Burn, P. L.; Meredith, P. *Appl. Phys. Lett.* **2011**, *98*, No. 153301.

(13) Lin, L.-Y.; Tsai, C.-H.; Wong, K.-T.; Huang, T.-W.; Wu, C.-C.; Chou, S.-H.; Lin, F.; Chen, S.-H.; Tsai, A.-I. *J. Mater. Chem.* **2011**, *21*, 5950.

(14) Jørgensen, M.; Krebs, F. C. *J. Org. Chem.* **2005**, *70*, 6004.

(15) (a) Wu, I.-Y.; Lin, J. T.; Tao, Y.-T.; Balasubramaniam, E.; Su, Y. Z.; Ko, C.-W. *Chem. Mater.* **2001**, *13*, 2626. (b) Evans, R.; Gupta, A. PCT Int. Appl. 132,952 A1, 2010

(16) Ng, A. M. C.; Cheung, K. Y.; Fung, M. K.; Djurišić, A. B.; Chan, W. K. *Thin Solid Films* **2008**, *517*, 1047.

(17) Djurišić, A. B.; Fritz, T.; Leo, K. *J. Opt. A: Pure Appl. Opt.* **2000**, *2*, 458.

(18) Xue, J.; Rand, B. P.; Uchida, S.; Forrest, S. R. *Adv. Mater.* **2005**, *17*, 66.

(19) Lin, H.-W.; Lin, L.-Y.; Chen, Y.-H.; Chen, C.-W.; Lin, Y.-T.; Chiu, S.-W.; Wong, K.-T. *Chem. Commun.* **2011**, *47*, 7872.

(20) Sun, Y.; Takacs, C. J.; Cowan, S. R.; Seo, J. H.; Gong, X.; Roy, A.; Heeger, A. J. *Adv. Mater.* **2011**, *23*, 2226.

(21) Pettersson, L. A. A.; Roman, L. S.; Inganäs, O. *J. Appl. Phys.* **1999**, *86*, 487.

Quantum mechanical calculations:

The electronic and optical properties of **DTDCTB** have been estimated by density functional theory (DFT) and time-dependent DFT (TDDFT) calculations in CH_2Cl_2 solution using hybrid B3LYP function with the 6-31G(d) basis set, as implemented in the Gaussian09 (G09) program package.[1] The first electronic transition corresponds to a charge-transfer (CT) excitation from the ditolylaminothieny-localized HOMO to the LUMO, which is sizably populated on 2,1,3-benzothiadiazole and dicyanovinylene moieties (Table S1~2). The excitation energy of this lowest transition with the largest oscillator strength is calculated to be 1.84 eV (673.2 nm) (Figure S1), which is close to the observed experimental results. The second and third transitions may stem from two different $\pi \rightarrow \pi^*$ excitations from the HOMO-1 to the LUMO and from the HOMO to the LUMO+1.
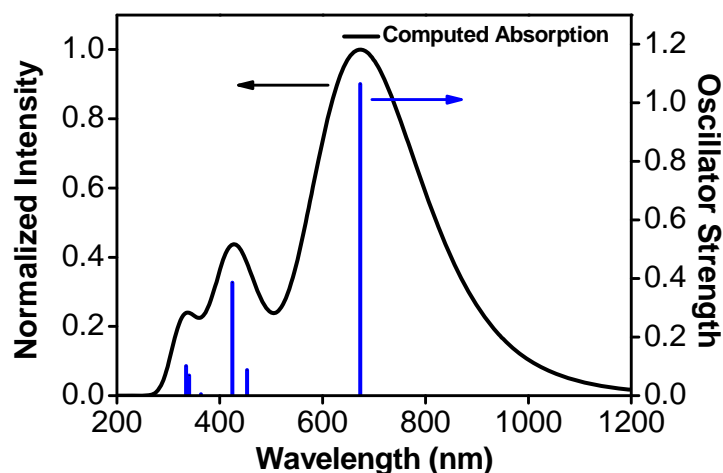
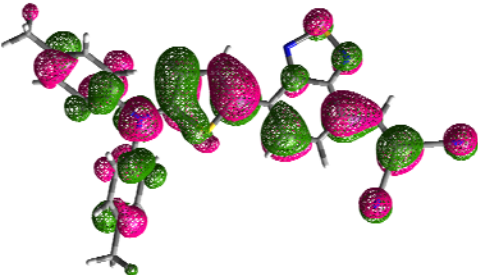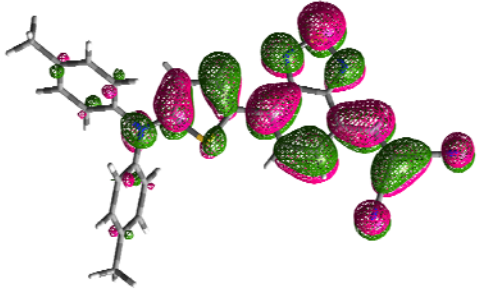**Figure S1.** Computed absorption spectrum of **DTDCTB** (oscillator strengths $f >$ 0.06).

[1] Censo, D. D.; Fantacci, S.; Angelis, F. D.; Klein, C.; Evans, N.; Kalyanasundaram, K.; Bolink, H. J.; Grätzel, M.; Nazeeruddin, M. K. *Inorg. Chem.* **2008**, *47*, 980.

Table S1. Calculated TDDFT Vertical Excitation Energies (eV, nm), Oscillator Strengths (*f*), Composition in Terms of Molecular Orbital Contributions, and Transition Characters[a]

Electronic Transition	*E* (eV, nm)	*f*	Composition	Character
S0 → S1	1.84 (673.2)	1.06	70% HOMO → LUMO	charge-transfer
S0 → S2	2.74 (454.2)	0.09	42% HOMO-1 → LUMO, 56% HOMO → LUMO+1	$\pi \to \pi^*$
S0 → S3	2.92 (424.4)	0.39	56% HOMO → LUMO+1, 41% HOMO-1 → LUMO	$\pi \to \pi^*$

[a] Within the considered energy range, we selectively calculate three transitions with moderate intensity ($f > 0.09$).

Table S2. Isodensity Surface Plots and Calculated Energy Levels of the HOMO and LUMO of DTDCTB

Orbital	Isodensity Surface Plot	Energy Level (eV)
HOMO		5.14
LUMO		3.13

PAPER

Efficient organic DSSC sensitizers bearing an electron-deficient pyrimidine as an effective π-spacer†

Li-Yen Lin,[a] **Chih-Hung Tsai,**[b] **Ken-Tsung Wong,**[*a] **Tsung-Wei Huang,**[b] **Chung-Chih Wu,**[*b] **Shu-Hua Chou,**[a] **Francis Lin,**[a] **Shinn-Horng Chen**[c] **and An-I Tsai**[c]

A series of new push–pull organic dyes incorporating electron-deficient pyrimidine as the π-spacer have been synthesized, characterized, and used as the sensitizers for dye-sensitized solar cells (DSSCs). In comparison with the model compound **M-TP**, which adopts phenylene as the π-spacer, the tailor-made dyes display enhanced spectral responses in the red portion of the solar spectrum. Through the introduction of two hexyloxy chains on the diphenylthienylamine donor, the DSSC employing dye **OHexDPTP** exhibited high power conversion efficiency up to 7.64% under AM1.5G irradiation.

Introduction

Dye-sensitized solar cells (DSSCs) have attracted considerable interest since Grätzel's pioneering report in 1991.[1] Photosensitizers certainly play a crucial role for highly efficient DSSCs and have been extensively investigated. In addition to Ru[II] polypyridyl-based sensitizers,[2] metal-free organic dyes have also been utilized in DSSCs because of the flexibility in tailoring their molecular structures, low cost, and high molar extinction coefficients.[3] Remarkably, organic-based DSSCs with conversion efficiencies comparable to the Ru-based DSSCs have been reported recently.[4] Due to the effective photoinduced intramolecular charge transfer characteristics, most of the efficient organic sensitizers are modeled on the donor–(π-spacer)–acceptor (D–π–A) system. For efficient solar energy conversion, it is desirable to use dyes that possess increased molar extinction coefficients that extend throughout the visible and into the near-IR regions. Organic sensitizers with long π-conjugated spacers had been shown to be operative in augmenting the molar extinction coefficients as well as in realizing panchromatic light-harvesting, giving moderate DSSC efficiency and stability.[4,5] In addition to the length of the π-conjugated spacer, the intrinsic electronic characteristics of the π-conjugated spacer may also affect the spectral response of the dyes. In most organic D–π–A dyes, the π-conjugated spacers linked to the acceptor

(cyanoacrylic acid) are typically electron-rich systems, such as thiophene derivatives,[6] furan,[7] selenophene,[8] and pyrrole.[9] However, such designs only yield limited bathochromic shifts in absorption. Meanwhile, a few organic D–π–A dyes incorporating electron-withdrawing terephthalonitrile[10] or electron-deficient heteroarenes such as quinoline,[11] isoxazole,[12] and thiazole[13] moieties as linkages to cyanoacrylic acid, showed more red-shifted absorption than their parent analogues and thus enhanced the light harvesting.

Here we report a series of organic D–π–A dyes, in which various diphenylthienylamines donors and cyanoacrylic acid acceptors are bridged by an electron-deficient pyrimidine ring. A model compound **M-TP** with phenylene as the π-spacer was also synthesized for parallel comparison. In general, the dyes were designed with the following three structural characteristics: (i) the pyrimidine-containing π-system which favors planar geometry necessary for effective intramolecular charge transfer;[14] (ii) the acceptor and also the TiO$_2$-anchoring group, cyanoacrylic acid, is linked to a highly electron-deficient pyrimidine ring; (iii) the diphenylthienylamine moiety is adopted as a stronger electron donor compared to the conventional triphenylamine moieties.[15] These three characteristics are all beneficial in lowering the energy of the intramolecular charge transfer transition. As a result, these dyes show evident bathochromic shifts in absorption, and thus effectively improve the light-harvesting range. To the best of our knowledge, this is the first time that the pyrimidine ring has been used as the π-conjugated spacer in organic photosensitizers for DSSCs.

Results and discussion

The synthetic pathways of new dyes **DPTP**, **OMeDPTP**, **OHexDPTP**, and model compound **M-TP** are illustrated in Scheme 1, and the detailed syntheses are described in the Experimental. Palladium-catalyzed Negishi coupling reactions of

[a]Department of Chemistry, National Taiwan University, Taipei, 10617, Taiwan. E-mail: kenwong@ntu.edu.tw; Fax: + 886-2-33661667; Tel: + 886-2-33661665

[b]Department of Electrical Engineering, Graduate Institute of Photonics and Optoelectronics, and Graduate Institute of Electronics Engineering, National Taiwan University, Taipei, 10617, Taiwan. E-mail: chungwu@cc.ee.ntu.edu.tw; Fax: +886-2-2367 1909; Tel: +886-2-3366 3636

[c]Energy Material Research Group, Eternal Chemical Co., Ltd., Kaohsiung, 821, Taiwan
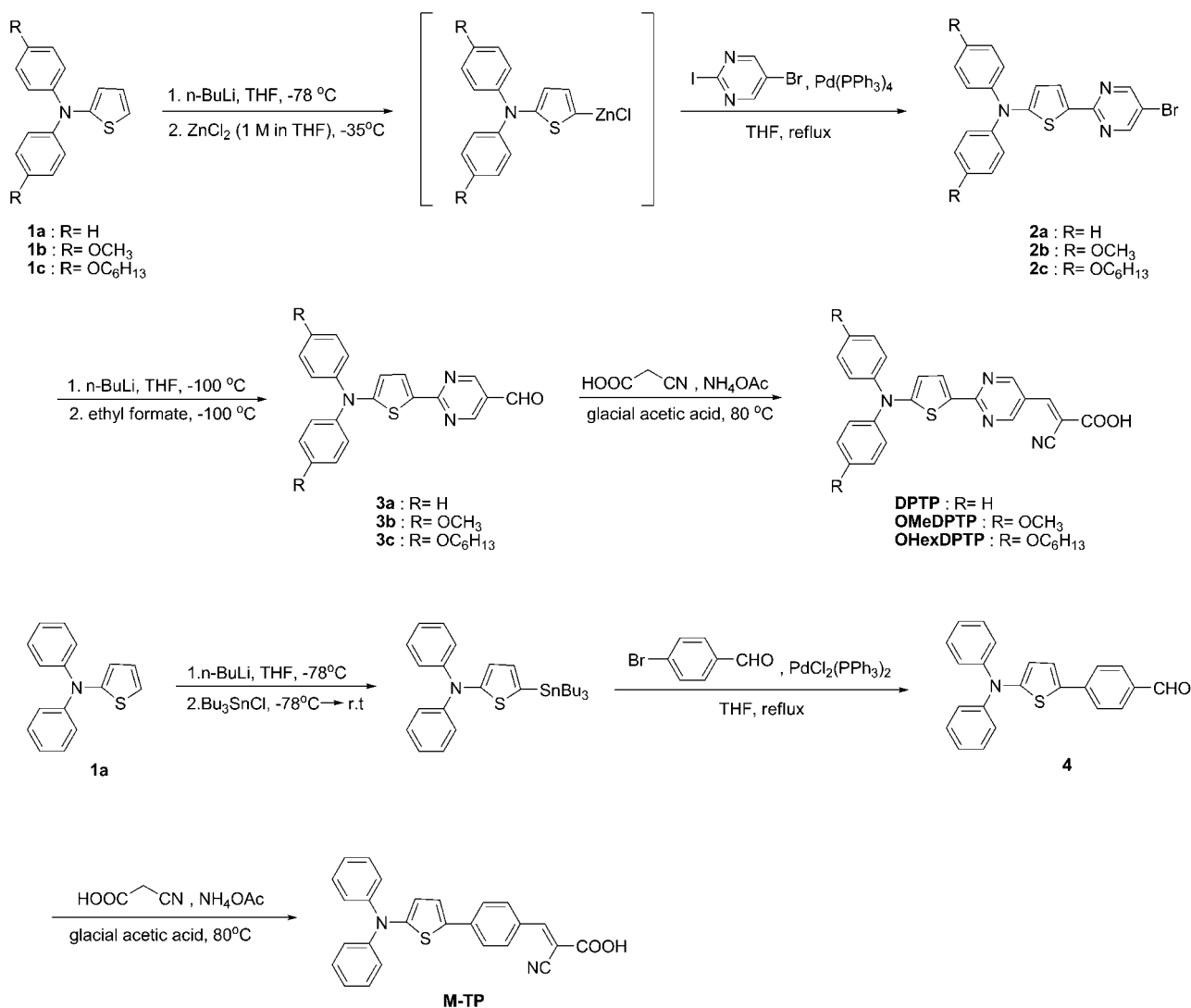
Scheme 1 Synthesis of dyes **DPTP**, **OMeDPTP**, **OHexDPTP**, and **M-TP**

1 with 5-bromo-2-iodopyrimidine afforded **2**, which were then converted to their corresponding carbaldehydes **3** by lithiation with *n*-butyl lithium and subsequently quenched with ethyl formate. Finally, the aldehydes were condensed with cyanoacetic acid to yield the target compounds **DPTP**, **OMeDPTP**, and **OHexDPTP** *via* the Knöevenagel reaction in the presence of ammonium acetate. The model compound **M-TP** was obtained *via* two-step processes that first involved the Stille coupling reaction of 5-(*N*,*N*-diphenylamino)-2-(tri-*n*-butylstannyl)thiophene with 4-bromobenzaldehyde, followed by the Knöevenagel condensation with cyanoacetic acid.

The UV-Vis absorption spectra and emission spectra of dyes in a *tert*-butanol–acetonitrile (1 : 1) solution are depicted in Fig. 1. Their photophysical data are also summarized in Table 1. The absorption spectrum of **DPTP** in solution shows an absorption maximum (λ_{max}) centered at 484 nm ($\varepsilon = 25300$ M^{-1} cm^{-1}), which is assigned to the π–π^* transition of the D–π–A conjugated system. The **M-TP** that incorporates phenylene as the π-spacer displays a weaker and blue-shifted absorption band at 438 nm ($\varepsilon = 19800$ M^{-1} cm^{-1}) in comparison with **DPTP**. It appears that
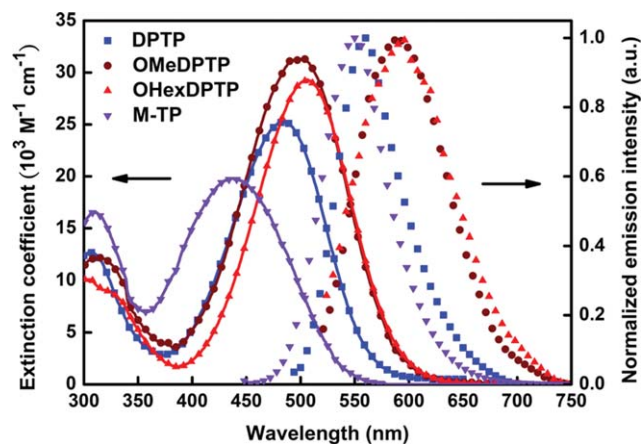

Fig. 1 Absorption (line + symbol) and emission (symbol) spectra of **DPTP**, **OMeDPTP**, **OHexDPTP**, and **M-TP** measured in a *tert*-butanol–acetonitrile (1 : 1) solution (10^{-5} M).

Table 1 Photophysical and electrochemical parameters of the dyes and adsorbed dye amount on TiO$_2$ nanoparticle films

Dye	$\lambda_{abs}{}^a$ (nm)	ε^a (M^{-1} cm^{-1})	$\lambda_{em}{}^a$ (nm)	λ_{abs} on TiO$_2{}^b$ (nm)	Γ^c (mol cm^{-2})	$E_{0-0}{}^d$ (V)	$E_{ox}{}^e$ (V)	$E_{ox}{}^{*f}$ (V)
DPTP	484	25300	560	454	1.8×10^{-7}	2.20	1.09	−1.11
OMeDPTP	502	31300	590	477	1.9×10^{-7}	2.11	0.99	−1.12
OHexDPTP	506	29300	594	467	6.0×10^{-8}	2.11	0.98	−1.13
M-TP	438	19800	549	409	2.5×10^{-7}	2.32	1.01	−1.31

^{a} Absorption and emission spectra were measured in a *tert*-butanol–acetonitrile (1 : 1, v/v) solution (10^{-5} M). ^{b} Absorption spectra on TiO$_2$ were obtained through measuring the dye adsorbed on 7 μm TiO$_2$ nanoparticle films in a chlorobenzene solution. ^{c} Γ is the surface density of the dye on the TiO$_2$ nanoparticle film. ^{d} E_{0-0} was estimated from the onset point of the absorption spectra. ^{e} The oxidation potentials of the dyes were measured in CH$_2$Cl$_2$ with 0.1 M tetrabutylammonium hexafluorophosphate (TBAPF$_6$) as electrolyte, scan rate: 100 mV s^{-1}; calibrated with ferrocene/ferrocenium (Fc/Fc$^+$) as an internal reference and converted to NHE by addition of 630 mV.[16] ^{f} $E_{ox}{}^* = E_{ox} - E_{0-0}$.

our molecular scaffold effectively shifts the absorption peak to a longer wavelength. Furthermore, **OMeDPTP** and **OHexDPTP** exhibit a λ_{max} at 502 ($\varepsilon = 31300$ M^{-1} cm^{-1}), and 506 nm ($\varepsilon = 29300$ M^{-1} cm^{-1}), respectively, which are red-shifted by *ca.* 20 nm compared to that of the parent dye **DPTP**, as a result of the stronger electron-donating nature of the dialkoxy substituents. **DPTP**, **OMeDPTP**, and **OHexDPTP** exhibit emission bands centered at 560, 590, and 594 nm, respectively, when excited on their absorption maxima.

Upon anchoring on the 7 μm porous TiO$_2$ nanoparticle films, the absorption of these dyes blue-shifted in comparison with those in the *tert*-butanol–acetonitrile (1 : 1) solution (Fig. 2). The blue shift may stem from the deprotonation of carboxylic acid upon adsorption onto the TiO$_2$ surface and the resulting carboxylate–TiO$_2$ unit is a weaker electron acceptor compared to the carboxylic acid.[6g] Similarly to many metal-free dyes,[6g,7,13,17] the absorption of the dyes exhibit negative solvatochromism, *i.e.* a blue shift of λ_{max} in polar solvents (see Fig. 3, taking **DPTP** as an example). This phenomenon may be attributed to the interaction of polar solvent molecules with the carboxylic acid, which decreases the electron-withdrawing strength of the COOH group.

Density function theory (DFT) calculations show a coplanar conformation between thiophene and pyrimidine due to the lack of *ortho–ortho* steric interactions, and the HOMOs of both sensitizers are mainly populated on diphenylamine and thiophene moieties, whereas LUMOs are sizably delocalized through pyrimidine and cyanoacrylic acid fragments (Fig. 4). This result suggests that the HOMO–LUMO excitation would shift the electron density distribution from the diphenylamine unit to the cyanoacrylic acid moiety, facilitating efficient photoinduced/interfacial electron injection from excited dyes to the TiO$_2$ electrode.

Quasi-reversible oxidation waves (E_{ox} in Table 1) of the dyes were observed in the cyclic voltammetry (CV), which can be attributed to the oxidation of the diphenylthienylamine moieties. The lower oxidation potential of **OMeDPTP** and **OHexDPTP** *vs.* **DPTP** can be ascribed to the presence of stronger electron-donating dialkoxy substituents. The zero–zero excitation energy (E_{0-0}), which was estimated from the onset point of the absorption spectra, and the ground-state oxidation potential (E_{ox}) were used to calculate the excited-state oxidation potential $E_{ox}{}^* (= E_{ox} - E_{0-0})$. It is worth mentioning that both ground-state and excited-state oxidation potentials of **DPTP** are more positive than those of **M-TP**, yet the difference in the excited-state oxidation potentials of the two dyes is larger than that in ground-state oxidation potentials. It clearly suggests that the introduction of the electron-deficient pyrimidine as the π-spacer has a significant influence on the excited-state potential but a more limited effect on the ground-state oxidation potential of **DPTP**. The different influence on the ground-state and excited-state oxidation potentials by incorporating pyrimidine leads to a narrow energy gap of **DPTP**. The deduced $E_{ox}{}^*$ values of these dyes are more negative than the conduction band edge of the
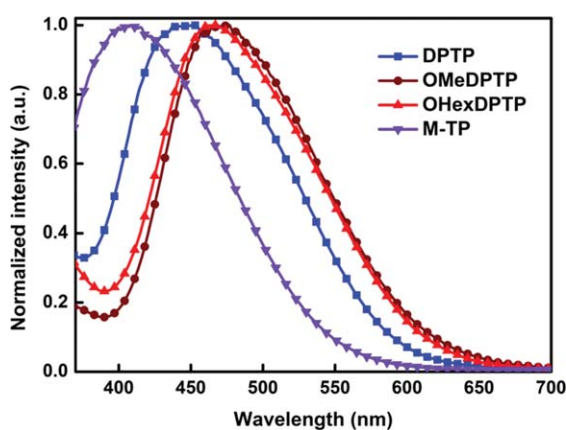
Fig. 2 Absorption spectra of the dyes anchoring on the 7 μm porous TiO$_2$ nanoparticle films.
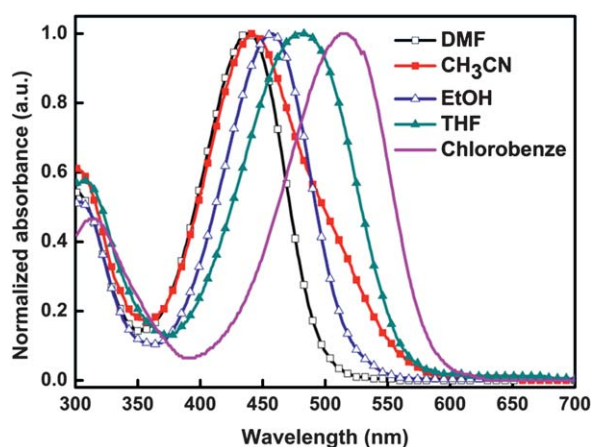
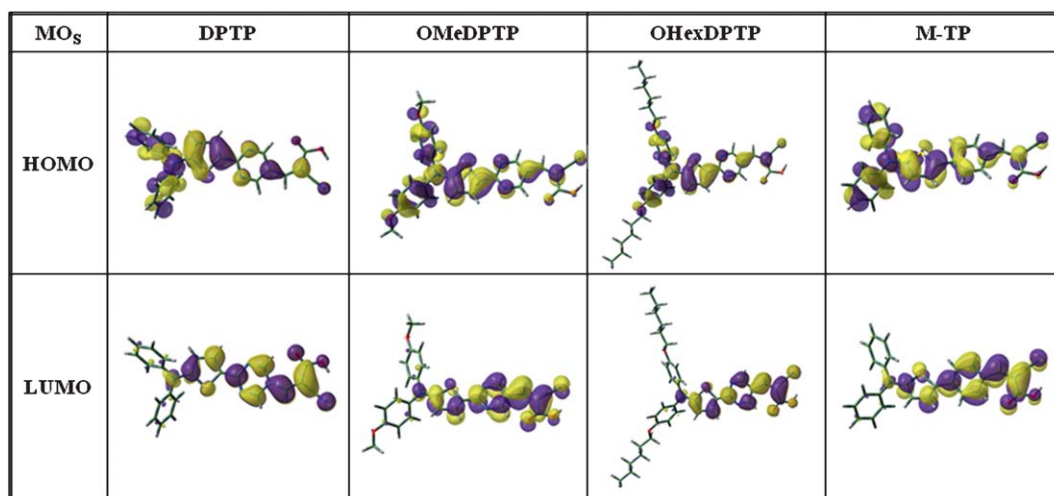**Fig. 3** Absorption spectra of **DPTP** in different solvents.

Fig. 4 Frontier molecular orbitals (HOMO and LUMO) of the dyes calculated with DFT on a B3LYP/6-31G(d) level.

TiO$_2$ (-0.5 V *vs.* NHE),[18] indicating that the electron injection process shall be energetically favorable. In addition, the ground-state oxidation potentials of the dyes are more positive than the redox potential of the iodide/triiodide couple (0.4 V *vs.* NHE), suggesting that the oxidized dyes shall be able to accept electrons from I$^-$ thermodynamically for effective dye regeneration and minimize the charge recombination between oxidized dyes and photoinjected electrons in TiO$_2$.

The photovoltaic characteristics of these dyes as the sensitizers for DSSCs were evaluated with a sandwich DSSC cell using 0.6 M 1-butyl-3-methylimidazolium iodide (BMII), 0.05 M LiI, 0.03 M I$_2$, 0.5 M 4-*tert*-butylpyridine, and 0.1 M guanidinium thiocyanate in a mixture of acetonitrile–valeronitrile (85 : 15, v/v) as the redox electrolyte (details of the device preparation and characterization are described in the experimental). The incident monochromatic photon-to-current conversion efficiency (IPCE) spectra and the current–voltage (*J–V*) curves under standard global AM 1.5 solar irradiation of the DSSCs are plotted in Fig. 5 and Fig. 6, respectively. The DSSCs using **DPTP**, **OMeDPTP**, and **OHexDPTP** show IPCEs > 70% from 380–400 nm to 570 nm and IPCE maxima of 90–92% around

450 nm, indicating highly efficient DSSC performances. In agreement with the trend in absorption spectra, the IPCE spectra of **DPTP**, **OMeDPTP** and **OHexDPTP** all exhibit higher peak values and extend to longer wavelengths than that of the model compound **M-TP**. Moreover, with dialkoxy substituents, IPCE spectra of **OMeDPTP** and **OHexDPTP** extend to longer wavelengths than that of **DPTP**. As listed in Table 2, the short-circuit photocurrent density (J_{sc}), open-circuit voltage (V_{oc}), and fill factor (*FF*) of the **OHexDPTP** cell are 13.79 mA cm^{-2}, 0.77 V, and 0.72, respectively, yielding an overall conversion efficiency (η) of 7.64%. Although both **DPTP** and **OMeDPTP** cells possess J_{sc} similar to (or even slightly higher than) that of the **OHexDPTP** cell, yet with relatively lower V_{oc}, they both exhibit inferior η values of 6.72% and 7.05%, respectively. For a fair comparison, the **N719**-sensitized DSSC was also fabricated and tested under similar conditions (Table 2). The efficiency of the **OHexDPTP** cell reaches ~90% of the **N719** cell efficiency.

Interestingly, **DPTP** and **OHexDPTP** show nearly the same J_{sc} despite the larger molar extinction coefficient and more red-shifted absorption of **OHexDPTP**. This is likely to be due to the smaller density of **OHexDPTP** adsorbed on the TiO$_2$ surface
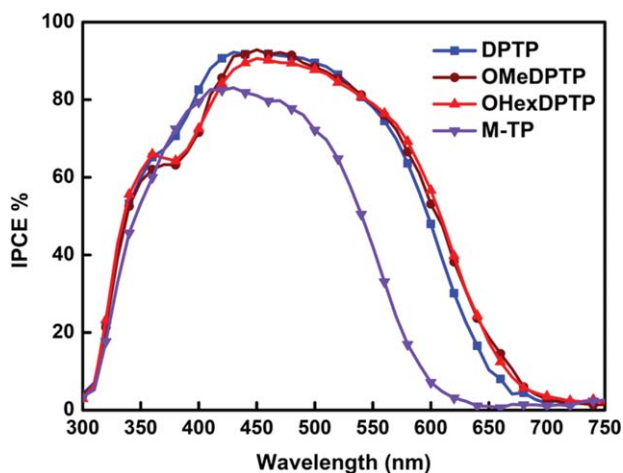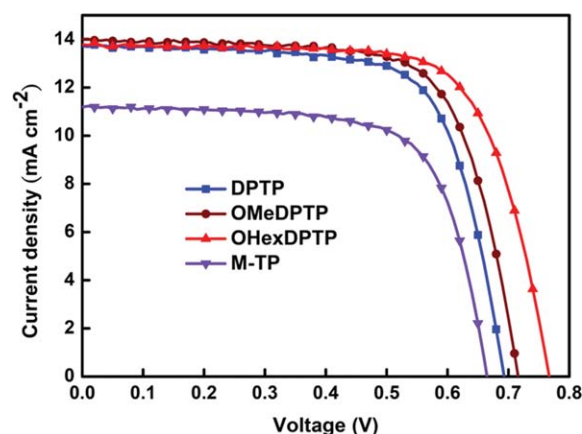

Fig. 5 IPCE spectra of DSSCs.

Fig. 6 Photocurrent density *vs.* voltage for DSSCs under AM1.5G simulated solar light (100 mW cm^{-2}).

Table 2 DSSC performance parameters.[a]

Dye	J_{sc} (mA cm^{-2})	V_{oc} (V)	FF	η (%)
DPTP	13.72	0.69	0.71	6.72
OMeDPTP	14.01	0.71	0.71	7.05
OHexDPTP	13.79	0.77	0.72	7.64
M-TP	11.19	0.66	0.70	5.22
N719	16.12	0.76	0.70	8.57

[a] The concentration of the organic dyes was maintained at 0.5 mM in chlorobenzene solution, with 0.5 mM deoxycholic acid (DCA) as a co-adsorbent [N719 was fabricated in *tert*-butanol–acetonitrile (1 : 1, v/v) solution under the same conditions]. Performances of DSSCs were measured with a 0.125 cm^2 working area. Irradiating light: AM1.5G (100 mW cm^{-2}).

Fig. 7 Electrochemical impedance spectroscopy (a) Nyquist plots; (b) Bode phase plots for DSSCs based on **DPTP**, **OMeDPTP**, and **OHexDPTP** dyes.

with greater steric congestion of the dihexyloxy-substituted diphenylthienylamine moiety at the donor. By desorbing the dyes adsorbed onto the TiO$_2$ surface with basic solution, the adsorbing densities were determined to be 1.8×10^{-7} and 6.0×10^{-8} mol cm^{-2} for **DPTP** and **OHexDPTP**, respectively, supporting such a mechanism. On the other hand, the surface density of **OMeDPTP** is similar to that of **DPTP** due to their similar molecular sizes, and thus the largest J_{sc} of **OMeDPTP** among the dyes can be ascribed to its simultaneously better light-harvesting ability and larger surface density on TiO$_2$.

Through the introduction of two long aliphatic hexyloxy chains on the diphenylthienylamine donor, one also notes that the **OHexDPTP**-based cell gives an enhanced V_{oc} in contrast to the **DPTP**- and **OMeDPTP**-based cells. Electrochemical impedance spectroscopy (EIS) was conducted to elucidate these phenomena. In this study, the impedance spectroscopy was carried out by subjecting the cell to the constant AM1.5G 100 mW cm^{-2} illumination and to the bias at the open-circuit voltage V_{oc} of the cell (namely, under the condition of no dc electric current), for better manifesting the process at the TiO$_2$/electrolyte interface of a cell under operation.[19] Fig. 7a shows the EIS Nyquist plots (*i.e.* minus imaginary part of the impedance $-Z''$ *vs.* the real part of the impedance Z' when sweeping the frequency) for DSSCs based on **DPTP**, **OMeDPTP** and **OHexDPTP** dyes. For the frequency range investigated (20 Hz to 1 MHz), in all cells, a larger semicircle occurs in the lower frequency range (~20 Hz to 1 kHz) and a smaller semicircle occurs in the higher frequency range. With the bias illumination and voltage applied, the larger semicircle at lower frequencies corresponds to the charge transfer processes at the TiO$_2$/dye/electrolyte interface, while the smaller semicircle at higher frequencies corresponds to the charge transfer processes at the Pt/electrolyte interface. The three cells hardly show any difference in smaller semicircles at higher frequencies, but the difference in larger semicircles at lower frequencies between the **OHexDPTP** and **DPTP** (or **OMeDPTP**) cells is significant. The larger width of the lower-frequency semicircle of the **OHexDPTP** cell indicates a larger charge-transfer resistance at the TiO$_2$/dye/electrolyte interface.

Fig. 7b shows the EIS Bode plots (*i.e.* the phase of the impedance *vs.* the frequency) of the DSSCs based on **DPTP**, **OMeDPTP**, and **OHexDPTP** dyes. For the frequency range investigated, both EIS Bode plots also exhibit two peak features; the one at higher frequencies corresponds to the charge transfer
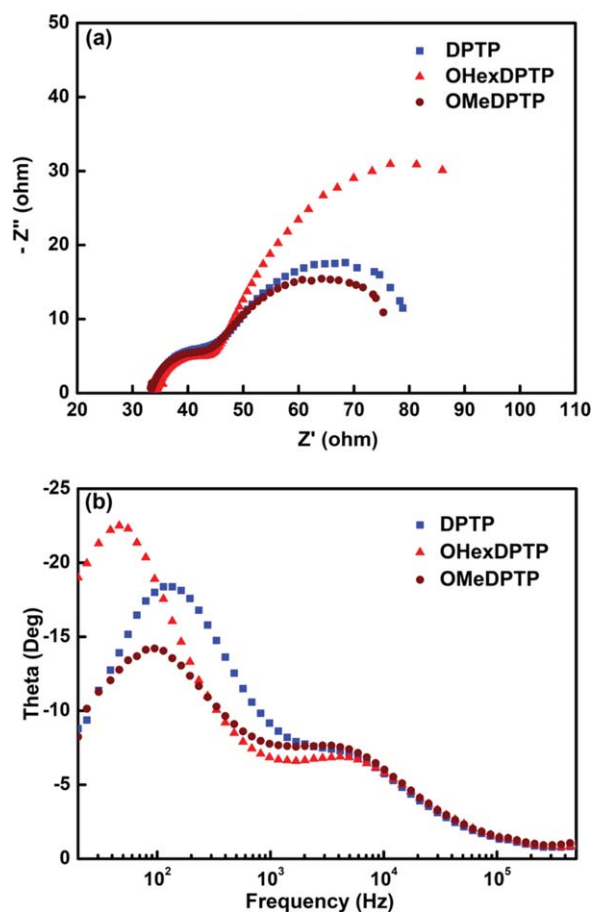
at the Pt/electrolyte interface, and the one at lower frequencies corresponds to the charge transfer at the TiO$_2$/dye/electrolyte interface. Again, the difference in Bode plots of the three cells mainly occurs in the lower-frequency range. The characteristic frequency of the lower-frequency peak in the Bode plot is related to the charge recombination rate, and its reciprocal is associated with the electron lifetime.[20] As can be seen in Fig. 7b, the lower-frequency peak of the **OHexDPTP** cell shifts to a significantly lower frequency (compared to the **DPTP** and **OMeDPTP** cells), indicating that the electron lifetime was effectively prolonged by the two longer hexyloxy chains near the TiO$_2$/dye/electrolyte interface. EIS results clearly suggest that the two longer hexyloxy chains of **OHexDPTP** act as effective blocking units between the TiO$_2$ surface and the electrolyte, preventing hydrophilic I$_3^-$ ions approaching the TiO$_2$ surface and thereby leading to suppressed charge recombination/dark current and lengthened electron lifetimes.[21] These factors may in turn lead to the higher V_{oc} of the **OHexDPTP** cell than those of the **DPTP** and **OMeDPTP** cells.

Conclusions

In summary, a series of new push–pull (D–π–A) DSSC sensitizers have been synthesized and characterized, in which different diphenylthienylamines bearing various terminal substituents

were chosen as donor (D) that were bridged by electron-deficient pyrimidine rings to the acceptor (A), cyanoacrylic acid. By taking advantage of the characteristic planarity and electronic deficiency of pyrimidine, the new dyes efficiently yield the bathochromic shift in absorption and effectively improve the light-harvesting. The introduction of two long hexyloxy chains on the diphenylthienylamine donor appears to suppress charge recombination at the TiO$_2$/dye/electrolyte interface, leading to a higher open-circuit voltage of the solar cell. A solar cell device based on the sensitizer **OHexDPTP** yielded an overall conversion efficiency of 7.64% under AM1.5G irradiation. This new molecular design strategy could trigger the future development of other simple organic photosensitizers for efficient DSSCs.

Experimental

Synthesis and materials

All chemicals and reagents were used as received from commercial sources without purification. Solvents for chemical synthesis were purified by distillation. All chemical reactions were carried out under an argon or nitrogen atmosphere. The starting materials 2-(N,N-diphenylamino)thiophene (**1a**),[22] 2-[N,N-bis(4-methoxyphenyl)amino]thiophene (**1b**),[23] 2-[N,N-bis-(4-hexyloxyphenyl)amino]thiophene (**1c**),[23] 5-bromo-2-iodo-pyrimidine,[24] and 5-(N,N-diphenylamino)-2-(tri-n-butylstannyl)thiophene[22] were synthesized according to the published procedures.

Synthesis of [5-(5-bromo-pyrimidin-2-yl)-thiophen-2-yl]-N,N-diphenylamine (2a). To a stirring solution of **1a** (5.03 g, 20 mmol) in anhydrous THF (60 mL) was added dropwise to n-BuLi (1.6 M, 13.13 mL, 21 mmol) at −78 °C under an argon atmosphere. The reaction mixture was warmed to −35 °C and stirred for 15 min. ZnCl$_2$ (22 mL of a 1 M solution in THF, 22 mmol) was then added to the reaction mixture in one portion, then the reaction mixture was warmed to room temperature and stirred for 30 min. To the above resulting zinc reagent, 5-bromo-2-iodopyrimidine (5.70 g, 20 mmol), Pd(PPh$_3$)$_4$ (1.15 g, 1 mmol), and THF (80 mL) was added. The whole mixture was heated to reflux under argon for 3 h. After cooling to room temperature, the reaction mixture was poured into water and extracted with ethyl acetate, the combined extracts were washed with brine, dried over anhydrous magnesium sulfate, and filtered. The solvent was removed by rotary evaporation, and the crude product was purified by column chromatography on silica gel with dichloromethane/hexane (v/v, 1 : 1) as eluent to afford **2a** as a yellow solid (5.83 g, 71% yield). M.p. 160–162 °C; IR (KBr) ν 3068, 3028, 1587, 1547, 1468, 1293, 1120, 810 cm^{-1}; ^{1}H NMR (CD$_2$Cl$_2$, 400 MHz) δ 8.59 (s, 2H), 7.74 (d, J = 4.0 Hz, 1H), 7.33 (t, J = 7.6 Hz, 4H), 7.24 (d, J = 7.6 Hz, 4H), 7.14 (t, J = 7.6 Hz, 2H), 6.53 (d, J = 4.0 Hz, 1H); ^{13}C NMR (CD$_2$Cl$_2$, 100 MHz) δ 159.8, 158.0, 157.8, 147.4, 131.6, 129.9, 129.8, 124.9, 124.6, 117.4, 115.9; HRMS (m/z, FAB$^+$) Calcd. for C$_{20}$H$_{14}$^{79}BrN$_3$S 407.0092, found 407.0102. Calcd. for C$_{20}$H$_{14}$^{81}BrN$_3$S 409.0071, found 409.0080.

Synthesis of [5-(5-bromo-pyrimidin-2-yl)-thiophen-2-yl]-N,N-bis(4-methoxyphenyl)amine (2b). The synthetic procedure was similar to that of **2a**, except that the eluent of column purification was dichloromethane/hexane (v/v, 3 : 4). **2b** was isolated as a yellow solid (56% yield). M.p. 145–147 °C; IR (KBr) ν 3071, 3020, 2958, 2837, 1606, 1550, 1298, 1168, 1030, 829 cm^{-1}; ^{1}H NMR (CD$_2$Cl$_2$, 400 MHz) δ 8.53 (s, 2H), 7.65 (d, J = 4.0 Hz, 1H), 7.21 (dd, J = 2.4, 6.8 Hz, 4H), 6.88 (dd, J = 2.4, 6.8 Hz, 4H), 6.24 (d, J = 4.0 Hz, 1H), 3.80 (s, 6H); ^{13}C NMR (CD$_2$Cl$_2$, 100 MHz) δ 160.6, 160.1, 157.7, 157.5, 140.4, 130.5, 127.9, 126.8, 115.1, 115.0, 112.0, 56.0; HRMS (m/z, FAB$^+$) Calcd. for C$_{22}$H$_{18}$^{79}BrN$_3$O$_2$S 467.0303, found 467.0299. Calcd. for C$_{22}$H$_{18}$^{81}BrN$_3$O$_2$S 469.0283, found 469.0281.

Synthesis of [5-(5-bromo-pyrimidin-2-yl)-thiophen-2-yl]-N,N-bis(4-hexyloxyphenyl)amine (2c). The synthetic procedure was similar to that of **2a**, except that the eluent of column purification was dichloromethane/hexane (v/v, 2 : 3). **2c** was isolated as a yellow solid (81% yield). M.p. 86–88 °C; IR (KBr) ν 3040, 2954, 2856, 1605, 1547, 1240, 1009, 821 cm^{-1}; ^{1}H NMR (CDCl$_3$, 400 MHz) δ 8.53 (s, 2H), 7.67 (d, J = 4.0 Hz, 1H), 7.20 (dd, J = 2.0, 6.8 Hz, 4H), 6.85 (dd, J = 2.0, 6.8 Hz, 4H), 6.27 (d, J = 4.0 Hz, 1H), 3.94 (t, J = 6.8 Hz, 4H), 1.79 (m, 4H), 1.47 (m, 4H), 1.35 (m, 8H), 0.93 (t, J = 6.8 Hz, 6H); ^{13}C NMR (CDCl$_3$, 100 MHz) δ 160.3, 159.6, 157.1, 156.4, 139.7, 130.1, 127.0, 126.3, 115.2, 114.2, 111.5, 68.2, 31.7, 29.3, 25.8, 22.7, 14.2; HRMS (m/z, FAB$^+$) Calcd. for C$_{32}$H$_{38}$^{79}BrN$_3$O$_2$S 607.1868, found 607.1862. Calcd. for C$_{32}$H$_{38}$^{81}BrN$_3$O$_2$S 609.1848, found 609.1843.

Synthesis of 2-(5-N,N-diphenylaminothiophen-2-yl)-pyrimidine-5-carbaldehyde (3a). To a stirring solution of **2a** (4.90 g, 12 mmol) in 160 mL anhydrous THF was added dropwise to n-BuLi (1.6 M, 7.73 mL, 12.36 mmol) at −100 °C under an argon atmosphere. The resulting solution was stirred for 20 min, after which dry ethyl formate (1.03 mL, 12.72 mmol) was added dropwise over 5 min. After stirring for 20 min, the reaction was quenched with 1.5 M HCl in THF solution (8 mL, 12 mmol). The cold bath was removed, and the reaction mixture was stirred for 2 h. The THF was removed under reduced pressure and the reaction mixture was extracted with chloroform, the combined extracts were washed with brine, dried over anhydrous magnesium sulfate, and filtered. The solvent was removed by rotary evaporation, and the crude product was purified by column chromatography on silica gel with dichloromethane/hexane (v/v, 2 : 1) as eluent to afford **3a** as an orange solid (1.33 g, 31% yield). M.p. 200–202 °C; IR (KBr) ν 3064, 2923, 2821, 1687, 1587, 1445, 1217, 1058, 835 cm^{-1}; ^{1}H NMR (CD$_2$Cl$_2$, 400 MHz) δ 9.94 (s, 1H), 8.90 (s, 2H), 7.90 (d, J = 4.4 Hz, 1H), 7.39–7.18 (m, 10H), 6.50 (d, J = 4.4 Hz, 1H); ^{13}C NMR (CD$_2$Cl$_2$, 100 MHz) δ 188.6, 164.4, 161.6, 158.8, 146.9, 133.1, 130.0, 129.7, 125.8, 125.4, 125.2, 115.5; HRMS (m/z, FAB$^+$) Calcd. for C$_{21}$H$_{15}$N$_3$OS 357.0936, found 357.0935.

Synthesis of 2-[5-N,N-bis(4-methoxyphenyl)aminothiophen-2-yl]-pyrimidine-5-carbaldehyde (3b). The synthetic procedure was similar to that of **3a**, and the eluent used for column purification was dichloromethane to afford **3b** as an orange solid (46% yield). M.p. 183–185 °C; IR (KBr) ν 3061, 3033, 2820, 2734, 1692, 1592, 1503, 1299, 1159, 825 cm^{-1}; ^{1}H NMR (CD$_2$Cl$_2$, 400 MHz) δ 9.89 (s, 1H), 8.84 (s, 2H), 7.84 (d, J = 4.4 Hz, 1H), 7.26 (dd, J = 2.4, 6.8 Hz, 4H), 6.91 (dd, J = 2.4, 6.8 Hz, 4H), 6.25 (d, J = 4.4 Hz, 1H), 3.81 (s, 6H);